Parallel implementation of the recursive Green's function method

P.S. Drouvelis [a,b,*], P. Schmelcher [a,c], P. Bastian [b]

[a] *Theoretische Chemie, Universität Heidelberg, Im Neuenheimer Feld 229, D-69120 Heidelberg, Germany*

[b] *Interdisziplinäres Zentrum für Wissenschaftliches Rechnen, Im Neuenheimer Feld 368, D-69120 Heidelberg, Germany*

[c] *Physikalisches Institut, Philosophenweg 12, Universität Heidelberg, D-69120 Heidelberg, Germany*

Abstract

A parallel algorithm for the implementation of the recursive Green's function technique, which is extensively applied in the coherent scattering formalism, is developed. The algorithm performs a domain decomposition of the scattering region among the processors participating in the computation and calculates the Schur's complement block in the form of distributed blocks among the processors. If the method is applied recursively, thereby eliminating the processors cyclically, it is possible to arrive at a Schur's complement block of small size and compute the desired block of the Green's function matrix directly. The numerical complexity due to the longitudinal dimension of the scatterer scales linearly with the number of processors, though, the computational cost due to the processors' cyclic reduction, establishes a bottleneck to achieve efficiency 100%. The proposed algorithm is accompanied by a performance analysis for two numerical benchmarks, in which the dominant sources of computational load and parallel overhead as well as their competitive role in the efficiency of the algorithm will be demonstrated.

Key words: Parallel recursive algorithm, Coherent transport, Recursive Green's function method, Schur's complement, Block tridiagonal matrices
PACS: 02.70.Bf, 73.23.Ad

* Corresponding author.
Email addresses: panos@tc.pci.uni-heidelberg.de (P.S. Drouvelis), peter@tc.pci.uni-heidelberg.de (P. Schmelcher), Peter.Bastian@iwr.uni-heidelberg.de (P. Bastian).

1 Introduction

In 1965, Gordon Moore predicted that the number of transistors packed on a chip would continue to double every year, a prediction known as the Moore's law [1]. During the past few decades, the rapid progress of novel experimental techniques, has resulted in scaling down the size of the integrated circuits on a chip according to Moore's law. Nowadays, chips with hundreds of millions of transistors have been industrially realised and are exploited in a wide range of commercial applications. However, the continuous scaling down in size of the transistors is about to reduce their dimensions thereby entering the mesoscopic regime, in which the electronic wave length becomes important, i.e., comparable with the size of the device, and quantum effects dominate and define the laws of information processing [2]. The natural route towards future electronics is therefore to understand these effects and comprehend them in the design of the nanoscaled devices. The necessary condition for the description of these phenomena in realistic mesoscopic transistors, regarding computational resources, is the ability to treat systems with million degrees of freedom.

The theoretical framework for the description of mesoscopic electronic transport has been established within the Landauer formalism [3], in which the conductance of a mesoscopic sample is in direct relation to the probability that an electron will transmit through it. To this end, several numerical techniques have been developed and applied to describe various physical setups. The most efficient method to attack coherent ballistic transport has proven to be the recursive Green's function (RGF) approach. The general framework for this approach can be found in Refs. [4,5,6] and depending on the emphasis of the individual scattering problem, alternative numerical techniques can be applied. Therefore, techniques such as the boundary element method [7], with an emphasis on the arbitrary geometry of the scattering region, or the modular Green's function method [8], in which the scattering region is initially decomposed in modules which are finally joined via the Dyson equation, have been developed to take into account the particular geometrical features of the scattering problem. Recently, a RGF technique has been applied to describe scanning probe experiments [9]. This technique describes tunneling, through the STM tip, which comprises the whole scattering area but scales equally well with the standard RGF method. As an alternative solution to improve the efficiency and consequently the capability to treat larger systems, approximations in the Schrödinger eigenvalue problem, as in the contact block reduction method [10], have been employed to treat multi-terminal three-dimensional problems with relatively good accuracy.

The aim of this paper is to present a parallel algorithm for the computation of the electronic transmission probability, within the framework of the RGF

method. The parallelization will allow us to treat large systems with millions of degrees of freedom and will be particularly efficient to handle highly complex modular scattering structures. The paper is organised as follows. In section 2 we discuss the basic guidelines of the coherent scattering formalism and the desired computational goal to be achieved. In section 3 we construct the parallel algorithm and calculate its numerical complexity. Section 4 contains an analysis of the performance and scalability of the applied parallel algorithm for certain numerical benchmarks. Finally, section 5 draws our main conclusions.

2 Basic guidelines of the coherent scattering formalism

Coherent scattering formalism implies that the conductance of a mesoscopic sample attached to two reservoirs (Fig. 1) is proportional to the quantum-mechanical probability $T(E)$ that an incoming electron at a Fermi energy E in the reservoirs will transmit through it. To evaluate the transmission probability $T(E)$ one has to solve the Schrödinger equation:

$$(E - H(\mathbf{r}) + i\eta)G^R(\mathbf{r};\mathbf{r}') = \delta(\mathbf{r} - \mathbf{r}') \tag{1}$$

where $H(\mathbf{r})$ is the Hamiltonian and $G^R(\mathbf{r};\mathbf{r}')$ is the retarded Green's function operators of the open system (scatterer + reservoirs). In the following we restrict ourselves to two-dimensional ($2D$) transport.

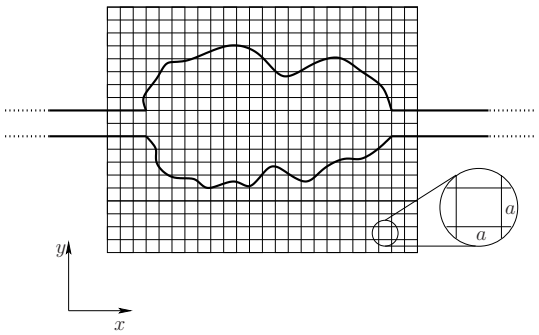

Fig. 1. Two-dimensional scattering region attached to two reservoirs discretized on a uniform lattice with constant a.

To proceed with the calculation of $T(E)$ we discretize our space on a uniform lattice with constant a. In order to represent the Hamiltonian operator $H(\mathbf{r})$ we use the tight-binding model assuming only nearest neighbor interactions [4]. In this case the Hamiltonian can be written:

$$\mathbf{H}(\mathbf{r}) = \sum_{\mathbf{r}} |\mathbf{r}\rangle \epsilon_{\mathbf{r}} \langle \mathbf{r}| + \sum_{\mathbf{r},\mathbf{\Delta r}} |\mathbf{r}\rangle V_{\mathbf{r},\mathbf{\Delta r}} \langle \mathbf{r} + \mathbf{\Delta r}| \tag{2}$$

where $\epsilon_{\mathbf{r}}$ is the on-site energy at the position $\mathbf{r} = (x, y)$ with $x = na$ and $y = ma$, $n, m \in \mathbb{N}$, $\mathbf{\Delta r}$ represents the vectors from $\mathbf{r}$ to their nearest neighbor sites and $V_{\mathbf{r},\mathbf{\Delta r}}$ is the nearest neighbor hopping energy. The dispersion relation for the $2D$ discretized lattice reads for a constant on-site energy:

$$E_{2D}(\mathbf{k}) = 4V_0 - 2V_0 cos(k_x a) - 2V_0 cos(k_y a) \tag{3}$$

where $\mathbf{k} = (k_x, k_y)$ is the electron's wavevector and $V_0 = -\hbar^2/(2m^* a^2)$ is the matrix hopping element linking each site to its nearest neighbor. In the limit $a \to 0$ we recover the usual parabolic relationship of a free particle in a continuum space.

The full tight-binding Hamiltonian of the open system (scatterer + reservoirs) can be then decomposed in the following block form:

$$\mathbf{H}(\mathbf{r}) = \begin{pmatrix} \mathbf{H_L} & \mathbf{V_L} & \mathcal{O} \\ \mathbf{V_L^\dagger} & \mathbf{H_S} & \mathbf{V_R} \\ \mathcal{O} & \mathbf{V_R^\dagger} & \mathbf{H_R} \end{pmatrix}$$

where the Hamiltonian $\mathbf{H_S}$ describes the electronic motion in an arbitrary scattering region which is coupled to two external reservoirs from the left and right, via the semi-infinite matrices $\mathbf{V_L}$ and $\mathbf{V_R}$ respectively. The Hamiltonian operators $\mathbf{H_L}$ and $\mathbf{H_R}$ are of infinite size and describe the electronic flow within the reservoirs.

Following Datta [2] one can accordingly partition the overall retarded Green's function operator of equation (1). It is then possible to obtain for the retarded Green's function operator of the scatterer the following expression,

$$\mathbf{G}(E) = [E\mathbf{I} - \mathbf{H_S} - \mathbf{\Sigma_R}(E) - \mathbf{\Sigma_L}(E)]^{-1} \tag{4}$$

which takes into account the effect of the coupling to the reservoirs, via the so called self-energy matrices $\mathbf{\Sigma_K}(E) = \mathbf{V_K^\dagger G_K}(E)\mathbf{V_K}$ due to the left ($\mathbf{K} = \mathbf{L}$) and right ($\mathbf{K} = \mathbf{R}$) reservoir. The function $\mathbf{G_K}$ is the retarded Green's function operator of the reservoir $\mathbf{K}$, i.e., $\mathbf{G_K}(E) = [(E + i\eta)\mathbf{I} - \mathbf{H_K}]^{-1}$.

Due to the tight-binding's model discretization, the space of the scattering region now consists of $n = 1, 2 \ldots, N$ slices along the x-direction each of which consists of $m = 1, 2, \ldots, M$ sites along the y-direction. The matrix $\mathbf{A} = E\mathbf{I} - \mathbf{H_S} - \mathbf{\Sigma_R}(E) - \mathbf{\Sigma_L}(E)$ we want to invert in order to evaluate $\mathbf{G}(E)$ is a $N \times N$ block tridiagonal matrix [4] whose elements are the blocks $\mathbf{A_{ij}}$ each

of which is of size $M \times M$:

$$\mathbf{A} = \begin{pmatrix} \mathbf{A_{11}} & \mathbf{A_{12}} & \mathcal{O} & \cdots & \mathcal{O} & \mathcal{O} & \mathcal{O} \\ \mathbf{A_{21}} & \mathbf{A_{22}} & \mathbf{A_{23}} & \cdots & \mathcal{O} & \mathcal{O} & \mathcal{O} \\ \mathcal{O} & \mathbf{A_{32}} & \mathbf{A_{33}} & \cdots & \mathcal{O} & \mathcal{O} & \mathcal{O} \\ \vdots & \vdots & \vdots & \ddots & \vdots & \vdots & \vdots \\ \mathcal{O} & \mathcal{O} & \mathcal{O} & \cdots & \mathbf{A_{N-2,N-2}} & \mathbf{A_{N-2,N-1}} & \mathcal{O} \\ \mathcal{O} & \mathcal{O} & \mathcal{O} & \cdots & \mathbf{A_{N-1,N-2}} & \mathbf{A_{N-1,N-1}} & \mathbf{A_{N-1,N}} \\ \mathcal{O} & \mathcal{O} & \mathcal{O} & \cdots & \mathcal{O} & \mathbf{A_{N,N-1}} & \mathbf{A_{N,N}} \end{pmatrix}$$

The expression for the evaluation of $T(E)$ can be given in a compact form within the Fisher-Lee relation [11]:

$$T(E) = Tr[\mathbf{\Gamma_R}(E)\mathbf{G}(E)\mathbf{\Gamma_L}(E)\mathbf{G}^{\dagger}(E)] \tag{5}$$

where $\mathbf{\Gamma_K}(E) = i[\mathbf{\Sigma_K}(E) - \mathbf{\Sigma_K^{\dagger}}(E)]$ is the strength of the coupling of the reservoir $\mathbf{K}$ to the scatterer. Due to the fact that the reservoirs are coupled only to the left and right of the scatterer, the blocks that correspond to the left interface of the scatterer with the lead, i.e. the upper left block $\sigma_{\mathbf{L}}(E)$ of $\mathbf{\Sigma_L}(E)$, and to the right interface of the scatterer with the lead, i.e. the down right block $\sigma_{\mathbf{R}}(E)$ of $\mathbf{\Sigma_R}(E)$, are the nonzero blocks of the matrices $\mathbf{\Sigma_K}(E)$. Therefore, the total self-energy due to the right and left reservoir has the following structure:

$$\mathbf{\Sigma_L}(E) + \mathbf{\Sigma_R}(E) = \begin{pmatrix} \sigma_{\mathbf{L}}(E) & \mathcal{O} & \mathcal{O} & \cdots & \mathcal{O} & \mathcal{O} & \mathcal{O} \\ \mathcal{O} & \mathcal{O} & \mathcal{O} & \cdots & \mathcal{O} & \mathcal{O} & \mathcal{O} \\ \mathcal{O} & \mathcal{O} & \mathcal{O} & \cdots & \mathcal{O} & \mathcal{O} & \mathcal{O} \\ \vdots & \vdots & \vdots & \ddots & \vdots & \vdots & \vdots \\ \mathcal{O} & \mathcal{O} & \mathcal{O} & \cdots & \mathcal{O} & \mathcal{O} & \mathcal{O} \\ \mathcal{O} & \mathcal{O} & \mathcal{O} & \cdots & \mathcal{O} & \mathcal{O} & \mathcal{O} \\ \mathcal{O} & \mathcal{O} & \mathcal{O} & \cdots & \mathcal{O} & \mathcal{O} & \sigma_{\mathbf{R}}(E) \end{pmatrix}$$

Due to the above mentioned structure of the self-energy matrices, it becomes clear that only the upper left block of $\mathbf{\Gamma_L}(E)$, $\gamma_{\mathbf{L}}(E) = i(\sigma_{\mathbf{L}}(E) - \sigma_{\mathbf{L}}^{\dagger}(E))$ and the down right block of $\mathbf{\Gamma_R}(E)$, $\gamma_{\mathbf{R}}(E) = i(\sigma_{\mathbf{R}}(E) - \sigma_{\mathbf{R}}^{\dagger}(E))$ are nonzero. Hence, the trace of the product of the four matrices occuring in equation (5) simplifies to:

$$T(E) = Tr[\gamma_{\mathbf{R}}(E)\mathbf{G_{1,N}}(E)\gamma_{\mathbf{L}}(E)\mathbf{G_{1,N}^{\dagger}}(E)] \tag{6}$$

Equation (6) implies that only the upper right block of the inverse of $\mathbf{A}$, $\mathbf{A^{-1}_{1,N}} = \mathbf{G_{1,N}}$ is necessary for the evaluation of $T(E)$. The ultimate goal is therefore to compute $\mathbf{A^{-1}_{1,N}}$.

3 The parallel algorithm

3.1 Prerequisites

The overall scattering problem, as discussed in section 2, is summarized to a $N \times N$ block tridiagonal matrix $\mathbf{A} = E\mathbf{I} - \mathbf{H} - \mathbf{\Sigma_R}(E) - \mathbf{\Sigma_L}(E)$ of which each block is of size $M \times M$, where the goal is to compute the upper right block of the inverse of $\mathbf{A}$, $\mathbf{A^{-1}_{1,N}}$.

The algorithm that we pursue should possess the following properties:

(1) Storage requirements should be restricted to a small number of blocks of size $M \times M$.
(2) The number of inversions and multiplications of the $M \times M$ blocks $\mathbf{A_{ij}}$, which scale as M^3, should be proportional to N. This corresponds to the numerical complexity of the sequential RGF technique in the asymptotic limit of large N and M:

$$C_{\text{seq}}(N, M) \approx NM^3$$

(3) Exploit the fact that the matrix $\mathbf{A}$ is Hermitian, i.e., for the off-diagonal blocks is claimed that $\mathbf{A^{\dagger}_{ij}} = \mathbf{A_{ji}}$.
(4) The algorithm should be parallelizable.

3.2 Preparations

3.2.1 Change of the inverse under permutation

Let $\mathbf{P_{ij}}$ be an elementary permutation matrix with the following properties:

(1) Set $\tilde{\mathbf{A}} = \mathbf{P_{ij}A}$, then $\tilde{\mathbf{A}}$ is identical to $\mathbf{A}$ except that rows i and j are interchanged.
(2) Set $\tilde{\mathbf{A}} = \mathbf{AP_{ij}}$, then $\tilde{\mathbf{A}}$ is identical to $\mathbf{A}$ except that columns i and j are interchanged.
(3) $\mathbf{P^T_{ij}} = \mathbf{P_{ij}} = \mathbf{P_{ji}}$.
(4) $\mathbf{P_{ij}} \cdot \mathbf{P^T_{ij}} = \mathbf{I}$, i.e., $\mathbf{P_{ij}}$ is orthogonal and self-inverse $\mathbf{P_{ij}} = \mathbf{P^{-1}_{ij}}$.

We call $\mathbf{P} = \mathbf{P_{i_n,j_n}} \dots \mathbf{P_{i_1,j_1}}$ a permutation matrix. Then $\mathbf{P^{-1}} = (\mathbf{P_{i_n,j_n}} \cdot \dots \cdot \mathbf{P_{i_1,j_1}})^{-1} = \mathbf{P^{-1}_{i_1,j_1}} \cdot \dots \cdot \mathbf{P^{-1}_{i_n,j_n}} = \mathbf{P_{i_1,j_1}} \cdot \dots \cdot \mathbf{P_{i_n,j_n}} = \mathbf{P^T}$. Now if we apply row and column permutations to the matrix $\mathbf{A}$, $\tilde{\mathbf{A}} = \mathbf{PAP^T}$ then for the inverse we have that $\tilde{\mathbf{A}}^{-1} = (\mathbf{PAP^T})^{-1} = \mathbf{P^{-T}A^{-1}P^{-1}} = \mathbf{PA^{-1}P^T}$.

The above imply the following two alternative paths for the computation of $\mathbf{A^{-1}_{1,N}}$:

(a) Starting from $\mathbf{A}$ we compute the inverse of it. Then by applying the appropriate row and column permutations, through operation of the permutation matrices, it is possible to shift the desired upper right block $\mathbf{A^{-1}_{1,N}}$ in another position of the inverse. Respectively, the down left block of $\mathbf{A}$ is also shifted. This first path can be illustrated graphically as follows:

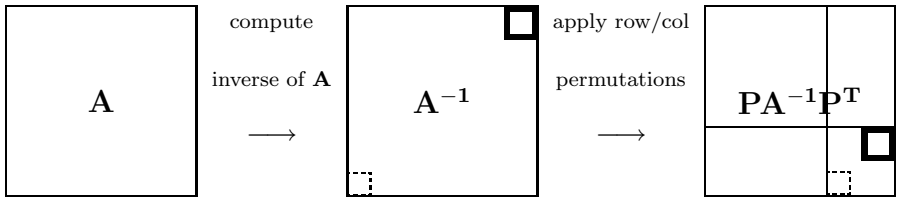

(b) Alternatively, if we start by applying row and column permutations in the initial matrix $\mathbf{A}$, then we can shift the upper right block $\mathbf{A_{1,N}}$ into another position. If we compute the inverse of the new matrix then the desired block $\mathbf{A^{-1}_{1,N}}$ will be located at the same position. Graphically, this second path implies:

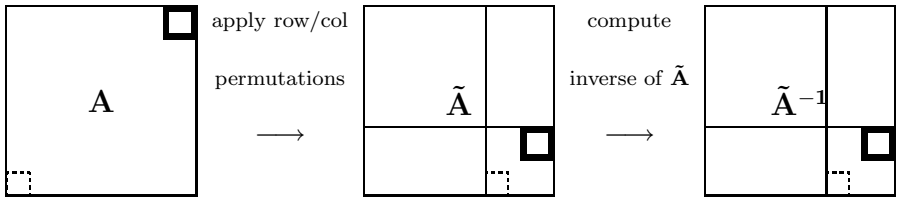

Therefore, the diagram implies that *computation of the desired block of the inverse matrix* $\mathbf{A^{-1}_{1,N}}$ *by following path (a) is equivalent to the computation of* $\mathbf{A^{-1}_{1,N}}$ *by following path (b)* .

3.2.2 Expression of the inverse via the Schur complement

Let any matrix $\mathbf{A}$ with a general 2×2 block structure:

$$\mathbf{A} = \begin{pmatrix} \mathbf{A_{11}} & \mathbf{A_{12}} \\ \mathbf{A_{21}} & \mathbf{A_{22}} \end{pmatrix}$$

Then the inverse of $\mathbf{A}$ in block form is:

$$\mathbf{A^{-1}} = \begin{pmatrix} \mathbf{A_{11}} + \mathbf{A_{11}^{-1}A_{12}S^{-1}A_{21}A_{11}^{-1}} & \mathbf{-A_{11}^{-1}A_{12}S^{-1}} \\ \mathbf{-S^{-1}A_{21}A_{11}^{-1}} & \mathbf{S^{-1}} \end{pmatrix}$$

where $\mathbf{S} = \mathbf{A_{22}} - \mathbf{A_{21}A_{11}^{-1}A_{12}}$ is the so called Schur's complement block.

Hence, together with the permutation Lemma (section 3.2.1) we arrive at the following statement:

If the block $\mathbf{A_{1,N}}$ *is transfered to the block* $\mathbf{A_{22}}$ *via permutation transformation then the desired block* $\mathbf{A_{1,N}^{-1}}$ *of the inverse can be obtained from the inverse* $\mathbf{S^{-1}}$ *of* $\mathbf{S}$.

3.3 Parallel recursive algorithm

To construct the parallel recursive algorithm for the computation of $\mathbf{A_{1,N}^{-1}}$ we proceed as follows. By starting from the matrix $\mathbf{A}$ in its original block tridiagonal form, we induce an additional block structure thereby distributing the domains of the scattering region to p processors as shown in Figure 2. This secondary level block structure, due to the scatterer's domain decomposition, consists of p blocks, which in turn contain $n_1, n_2, \ldots, n_p$ blocks respectively and $p + 1$ elementary blocks which correspond to the interface slices of the decomposed domains. Additionally, we encounter blocks that couple the interface slices with the p blocks corresponding to the scatterer's domains. The position of the upper right block $\mathbf{A_{1,N}^{-1}}$ that is required to be computed is indicated in Figure 2.

In the next step we reorder rows and columns, formally through permutation matrices, and we arrive at the reordered matrix with the structure of Figure 3. The reordered matrix has the 2×2 block structure,

$$\tilde{\mathbf{A}} = \begin{pmatrix} \mathbf{A^{II}} & \mathbf{A^{I\Gamma}} \\ \mathbf{A^{\Gamma I}} & \mathbf{A^{\Gamma\Gamma}} \end{pmatrix}$$

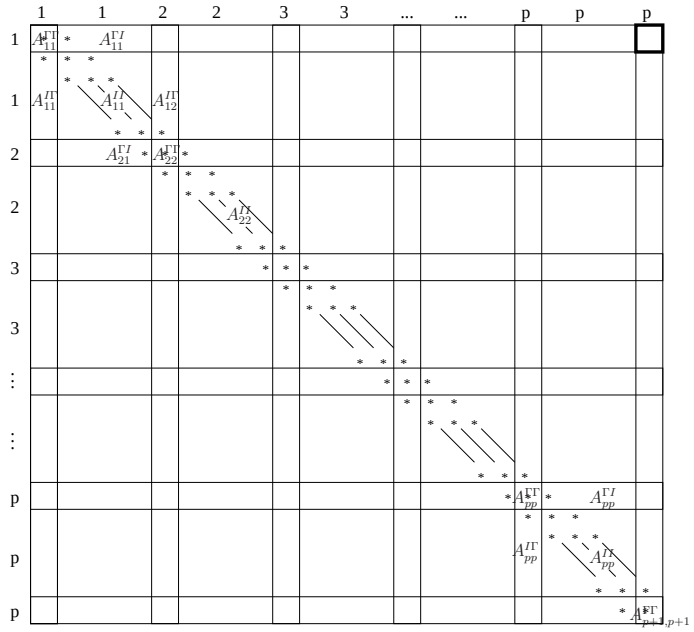

Fig. 2. Original block tridiagonal matrix with new secondary level block structure due to processor subdivision.

and moreover, the desired block to be computed is transfered to the upper right corner of $\mathbf{A^{\Gamma\Gamma}}$. Therefore, in order to compute $\mathbf{A^{-1}_{1,N}}$, it suffices to compute $\mathbf{S} = \mathbf{A^{\Gamma\Gamma}} - \mathbf{A^{\Gamma I}}(\mathbf{A^{II}})^{-1}\mathbf{A^{I\Gamma}}$ and extract the upper right block of $\mathbf{S^{-1}}$. The computation of $\mathbf{S}$ results again in a block tridiagonal matrix and the algorithm can be applied recursively, i.e., by knowing $\mathbf{S}$ and applying cyclic reduction among the processors which participate in $\mathbf{S}$, we can arrive recursively to a matrix that is small enough to compute $\mathbf{A^{-1}_{1,N}}$ directly.

Analytically, the stages to which the parallel RGF algorithm is divided as well as the corresponding numerical complexities are the following:

(1) First Stage: *Scatterer's domain decomposition and computation of* $\mathbf{S}$
The scatterer is decomposed in domains with $n_1, n_2, \ldots, n_k, \ldots, n_p$ blocks. Each domain corresponds to one of the altogether p processors participating in the computation and additionally, there are $p+1$ elementary blocks of each interface slice between the domains (Fig. 2). At this point we have to note that the last processor stores two interface blocks, i.e., $\mathbf{A^{\Gamma\Gamma}_{pp}}$ and $\mathbf{A^{\Gamma\Gamma}_{p+1,p+1}}$. Then we reorder rows and columns such that the matrix $\mathbf{A}$ has the block structure of Fig. 3. Subsequently, the algorithm performs a block Gaussian elimination adapted to the special sparse block structure of Fig. 3, i.e., it proceeds by eliminating $\mathbf{A^{\Gamma I}}$ using $\mathbf{A^{II}}$. Analytically, the steps of the block Gaussian elimination applied hereby:
$\forall$ processor k
for $i = 1 \ldots n_k$
$\mathbf{B} = (\mathbf{A^{II}_{kk}})^{-1}_{\mathbf{ii}}$

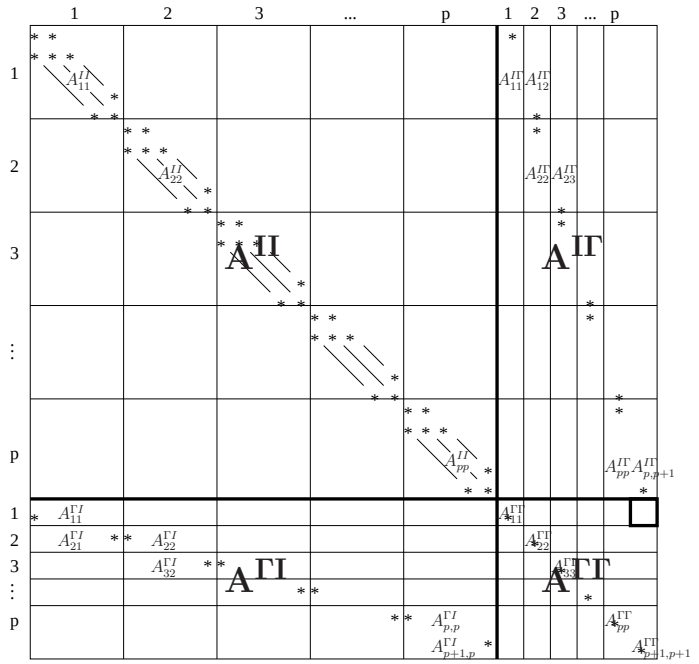

Fig. 3. Reordered matrix $\mathbf{A}$ after row and column permutations.

$(\mathbf{A^{II}_{kk}})_{\mathbf{i+1,i+1}} = (\mathbf{A^{II}_{kk}})_{\mathbf{ii}} - (\mathbf{A^{II}_{kk}})^{\dagger}_{\mathbf{i,i+1}} \mathbf{B} (\mathbf{A^{II}_{kk}})_{\mathbf{i,i+1}}$
$(\mathbf{A^{I\Gamma}_{kk}})_{\mathbf{i+1}} = -(\mathbf{A^{II}_{kk}})^{\dagger}_{\mathbf{i,i+1}} \mathbf{B} (\mathbf{A^{I\Gamma}_{kk}})_{\mathbf{i}}$
$(\mathbf{A^{\Gamma\Gamma}_{kk}})_{\mathbf{i+1}} = (\mathbf{A^{\Gamma\Gamma}_{kk}})_{\mathbf{i}} - (\mathbf{A^{I\Gamma}_{kk}})^{\dagger}_{\mathbf{i}} \mathbf{B} (\mathbf{A^{I\Gamma}_{kk}})_{\mathbf{i}}$

if $i == n_k + 1$

$\mathbf{B} = (\mathbf{A^{II}_{kk}})^{-1}_{\mathbf{n_k,n_k}}$
$\mathbf{A^{\Gamma\Gamma}_{kk}} = (\mathbf{A^{\Gamma\Gamma}_{kk}})_{\mathbf{n_k}} - (\mathbf{A^{I\Gamma}_{kk}})^{\dagger}_{\mathbf{n_k}} \mathbf{B} (\mathbf{A^{I\Gamma}_{kk}})_{\mathbf{n_k}}$
$\mathbf{A^{\Gamma\Gamma}_{k,k+1}} = -(\mathbf{A^{I\Gamma}_{kk}})^{\dagger}_{\mathbf{n_k}} \mathbf{B} \mathbf{A^{I\Gamma}_{k,k+1}}$

The numerical cost for each processor scales with n_p inversions of $M \times M$ blocks and requires $6 \cdot n_p$ multiplications of matrices (see the algorithm above). With respect to the storage only a few auxiliary blocks of size $M \times M$, independent of n_k, are required. Hence, each processor at the end of the first stage of the computation has stored the diagonal $\mathbf{A^{\Gamma\Gamma}_{k,k}}$ and off-diagonal $\mathbf{A^{\Gamma\Gamma}_{k,k+1}}$ block of the Schur complement. At this point we note that the notation used in the subscript of the blocks of $\mathbf{S}$ is identical to the one of the blocks of $\mathbf{A^{\Gamma\Gamma}}$ for convenience. The last processor computes, in addition to the two previously mentioned blocks, the last block $\mathbf{A^{\Gamma\Gamma}_{p+1,p+1}}$. The numerical complexity for each processor scales, in the limit of large N and M, with:

$$C_1 \approx 7 n_k M^3 \approx 7 \frac{N}{p} M^3$$

After the completion of the first stage, the Schur's complement block $\mathbf{S}$ has been computed with the form of distributed blocks $\mathbf{A^{\Gamma\Gamma}_{k,k}}$ and $\mathbf{A^{\Gamma\Gamma}_{k,k+1}}$ among the processors participating in the computation. Moreover, $\mathbf{S}$ has a block tridiagonal structure and is Hermitian:

$$\mathbf{S} = \begin{pmatrix} \mathbf{A_{11}^{\Gamma\Gamma}} & \mathbf{A_{12}^{\Gamma\Gamma}} & \mathcal{O} & \cdots & \mathcal{O} & \mathcal{O} & \mathcal{O} \\ \mathbf{A_{12}^{\Gamma\Gamma\dagger}} & \mathbf{A_{22}^{\Gamma\Gamma}} & \mathbf{A_{23}^{\Gamma\Gamma}} & \cdots & \mathcal{O} & \mathcal{O} & \mathcal{O} \\ \mathcal{O} & \mathbf{A_{23}^{\Gamma\Gamma\dagger}} & \mathbf{A_{33}^{\Gamma\Gamma}} & \cdots & \mathcal{O} & \mathcal{O} & \mathcal{O} \\ \vdots & \vdots & \vdots & \ddots & \vdots & \vdots & \vdots \\ \mathcal{O} & \mathcal{O} & \mathcal{O} & \cdots & \mathbf{A_{p-1,p-1}^{\Gamma\Gamma}} & \mathbf{A_{p-1,p}^{\Gamma\Gamma}} & \mathcal{O} \\ \mathcal{O} & \mathcal{O} & \mathcal{O} & \cdots & \mathbf{A_{p-1,p}^{\Gamma\Gamma\dagger}} & \mathbf{A_{p,p}^{\Gamma\Gamma}} & \mathbf{A_{p,p+1}^{\Gamma\Gamma}} \\ \mathcal{O} & \mathcal{O} & \mathcal{O} & \cdots & \mathcal{O} & \mathbf{A_{p,p+1}^{\Gamma\Gamma\dagger}} & \mathbf{A_{p+1,p+1}^{\Gamma\Gamma}} \end{pmatrix}$$

(2) Second Stage: *Cyclic reduction of the processors participating in the Schur's complement block*
To proceed further, we exploit the block tridiagonal structure of **S**. To this end we apply a recursive technique called cyclic reduction [12]. The implementation of this technique requires successive reordering of the processors in such a way that in each step the Schur's complement block is half the size as before. The first step of the cyclic reduction algorithm is shown in Fig. 4.

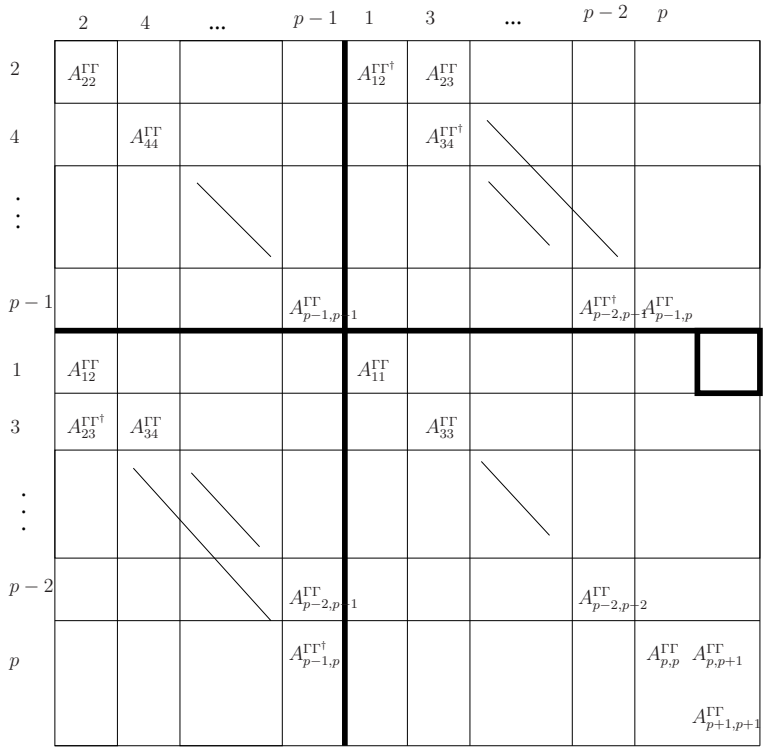

Fig. 4. Reordering according to the cyclic reduction algorithm for a Schur's complement block of size $(p+1)\times(p+1)$. The size of **S** after the applied block Gaussian elimination is reduced to half of the preceding size.

We observe that the reordered block structure possesses again the 2×2 structure of the matrix $\tilde{\mathbf{A}}$. Therefore by eliminating the off-diagonal block using the upper-diagonal, i.e., the procedure of the first stage, we arrive at a new Schur's complement block of half the size as the preceding one. By applying this procedure recursively, after $log_2(p)$ steps we arrive at a 3×3 block matrix, of which the upper-right diagonal block of the inverse is the desired $\mathbf{A}^{-\mathbf{1}}_{\mathbf{1,N}}$ one. At this point we should remark that in each recursive step, the first and the last processor should always participate in the new resulting Schur's complement block, as shown in Fig. 4. This condition ensures that the desired block $\mathbf{A}^{-\mathbf{1}}_{\mathbf{1,N}}$ is always located in the upper right corner of $\mathbf{S}$. In this second stage of parallelization, each recursive step requires one inversion and four multiplications for the calculation of the diagonal $\mathbf{A}^{\mathbf{\Gamma\Gamma}}_{\mathbf{kk}}$ and the fill-in $\mathbf{A}^{\mathbf{\Gamma\Gamma}}_{\mathbf{k,k+1}}$ blocks of the resulting Schur's complement block (see algorithm of the first stage applied to the block structure of Fig. 4). The numerical complexity of the second stage scales as:

$$C_2 \approx 5log_2(p)M^3$$

After $log_2(p)$ recursive steps, we are left with a 3×3 block matrix of which the first row, i.e., blocks $\mathbf{A}^{\mathbf{\Gamma\Gamma}}_{\mathbf{1,1}}$ and $\mathbf{A}^{\mathbf{\Gamma\Gamma}}_{\mathbf{1,2}}$, are stored in the first processor and the rest two rows, i.e., blocks $\mathbf{A}^{\mathbf{\Gamma\Gamma}}_{\mathbf{p,p}}$, $\mathbf{A}^{\mathbf{\Gamma\Gamma}}_{\mathbf{p,p+1}}$ (second row) and $\mathbf{A}^{\mathbf{\Gamma\Gamma}}_{\mathbf{p+1,p+1}}$ (third row), are stored in the last processor. The upper right block of the inverse of this 3×3 block matrix is the desired $\mathbf{A}^{-\mathbf{1}}_{\mathbf{1,N}}$ which can be straightforwardly computed.

(3) Third Stage: *Computation of the transmission coefficient*
At the last stage, there remain a few multiplications c of the blocks that are included inside the Fisher-Lee relation and are all known for the evaluation of $T(E)$. These operations are performed sequentially from the first processor. The numerical complexity for this last stage can be evaluated as,

$$C_3 \approx cM^3$$

and since c is a small constant, in the limit of large N, C_3 can be absorbed in C_1.

The numerical complexity of the parallel algorithm scales as:

$$C_{\text{par}}(N, M, p) \approx C_1 + C_2 + C_3 \approx 7\frac{N}{p}M^3 + 5log_2pM^3 \tag{7}$$

and the corresponding sequential ($p = 1$) one, as:

$$C_{\text{seq}}(N, M) \approx 7NM^3$$

We should remark that the algorithm developed here holds equally for scattering regions with complex boundary conditions, i.e., blocks $\mathbf{A_{ij}}$ with varying sizes, and can be generalized to the geometry of $3D$ scatterers in a straightforward manner.

4 Numerical benchmarks

4.1 Metrics for the analysis of performance and scalability

In this section an analysis of the performance and scalability for two specific numerical benchmarks will be pursued. This is required in order to test the models for the numerical complexity we derived so far and to demonstrate a measure for the capabilities and optimized use of the proposed algorithm. To proceed with such an analysis it is necessary to define some characteristic quantities for our parallel algorithm following Ref. [13]. Firstly, we define the problem size:

$$W(N, M) = 7NM^3$$

which is the number of numerical operations in the sequential algorithm ($p = 1$), i.e., the RGF approach, and is also equal to the serial run time T_s if a unit of time corresponds to each numerical operation. The cost of simulating the parallel algorithm on a single processor is:

$$pT_p(N, M, p) = pC_{\mathrm{par}}(N, M, p) = 7NM^3 + 5\,p\,log_2(p)M^3$$

where T_p is the parallel run time corresponding to $C_{\mathrm{par}}(N, M, P)$ if we assume a unit of time for each computational step. The overhead function T_0 of the parallel algorithm is defined as:

$$T_0(M, p) = pT_p - W = 5\,p\,log_2(p)M^3$$

and determines the part of its cost that is collectively spent by all processors compared to the sequential algorithm. The sources of overhead of a parallel system can be in general attributed to interprocessor communication, load imbalance and extra computational time due to a part of the program that is not parallelizable. In our algorithm the dominant contribution to the overhead results from the amount of operations during the cyclic elimination of the processors. The extra computational time required for the evaluation of the Fisher-Lee relation (this is the only not parallelizable part) can be neglected in

the limit of large N. As far as load imbalance is concerned, the two numerical benchmarks to be investigated will show a different significance of this source of overhead. Finally, we define the efficiency of the parallel algorithm as:

$$F = \frac{W}{pT_p} = \frac{7NM^3}{p\left(7\frac{N}{p}M^3 + 5\,log_2(p)M^3\right)} = \frac{1}{1 + \frac{5\,p\,log_2(p)}{7N}} \tag{8}$$

From this relation, we conclude that the efficiency is independent of the size of blocks M and depends only on the longitudinal length of the scatterer N and the number of processors p participating in the computation. Moreover, by scaling appropriately N with p, it is possible to maintain the efficiency fixed, a property met in scalable parallel algorithms. From Eq. (8) we can define the isoefficiency function:

$$W = KT_0$$

where $K = F/(1-F)$ is given for a specific F. For fixed K we can arrive at the following relation for N and K:

$$N = \frac{5}{7}Kp\,log_2(p) \tag{9}$$

Therefore, our algorithm can be cost-optimal if we choose $N = \frac{5}{7}Kp\,log_2(p)$ and scalable if we increase N with rate $O(p\,log_2(p))$. On the other hand, for a fixed size problem, i.e., keeping N and M fixed, we observe that the efficiency decreases with increasing p as a consequence of Amdahl's law (see Eq. (8)). Here some final remarks are in order. In the quantities defined so far, we have assumed lattices of unique size $N \times M$ for the discretization of the scattering regions (perfectly load balanced problems). In addition, the time spent for the interprocessor communications is neglected. This is due to the increased granularity of the block tridiagonal system, resulting in a better efficiency of the parallel algorithm.

4.2 Sinai billiard in a magnetic field

The first numerical benchmark to test the performance of our algorithm is the Sinai billiard in a homogeneous magnetic field. Figure 5 shows the setup. Modified Sinai billiard provide a class of systems for testing the correspondence between quantum and classical transport. Its simple geometry allows the use of lattices with a unique size for the discretization, leading therefore to a perfectly balanced problem with respect to the numerical work loaded to each

processor. It represents therefore an excellent ground to test the models for the complexity we developed in subsection 4.1.

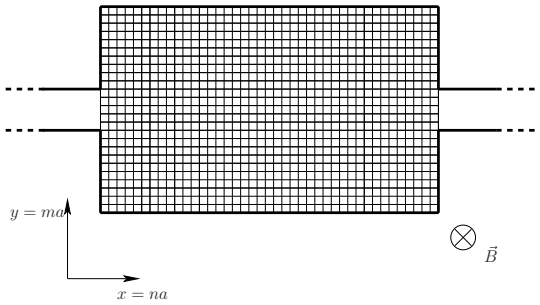

Fig. 5. Setup of a Sinai billiard attached to two reservoirs with $n = 0, 1, \ldots, N-1$ slices of $m = 0, 1, \ldots, M-1$ sites each, used in the fixed-size efficiency calculations. The ratio of the two dimensions is $\frac{N}{M} = \frac{8}{5}$.

The first setup to test the performance of our algorithm uses a 400×250 lattice for the discretization of the Sinai billiard (ten times resolved compared to the one of Figure 5). The first type of analysis consists of keeping the lattice fixed and studying the efficiency of the problem with increasing the number of processors. We remind the reader that the total cost of the parallel algorithm is dominated by the cost for the evaluation of the Schur's complement block and the cost due to the cyclic reduction of the processors (see Eq. (7)). Table 1 shows the times measured for the evaluation of $T(E, B)$ at a fixed energy E and magnetic field B.

Table 1
Measured time (Time) and efficiency (F) as a function of the number p of the processors for a Sinai billiard in a magnetic field with fixed size $N = 400$ and $M = 250$.

p	Time (sec)	$\_F\_$	p	Time (sec)	$\_F\_$	p	Time (sec)	$\_F\_$
1	1723.58	1.0	14	136.82	0.9	48	53.78	0.668
2	871.94	0.989	16	120.09	0.897	56	49.31	0.624
4	444.75	0.969	20	99.84	0.863	64	45.33	0.594
6	300.57	0.956	24	86.57	0.83	80	39.68	0.543
8	229.18	0.94	28	77.58	0.793	96	38.49	0.466
10	185.61	0.928	32	69.51	0.775	112	35.16	0.438
12	158.46	0.906	40	59.11	0.729	128	34.27	0.393

At this point we note that the system used for the time measurements has been a Linux cluster of 256 nodes with Dual AMD Athlon 1.4 GHz processors of 2 GB RAM each. Efficiency is 1.0 for $p = 1$ and gradually decreases with p. This is due to the fact that with increasing p, the term in equation (7) proportional

to $log_2(p)$, dominates with respect to the other term that decreases with $\frac{N}{p}$, thereby decreasing the efficiency of the proposed algorithm.

Figure 6 shows the efficiency F as a function of the number p of processors according to the performed time measurements (dots) compared to the analytical curve of Eq. (8). We observe that the agreement between the theoretical model and the measurements is very good. Therefore, we conclude that the dominant sources of numerical load have been succesfully identified and weighted. Further sources of overhead, such as the time required for interprocessors' communication, could be neglected as the work load is dominated by the amount of numerical operations that scale with M^3, i.e., multiplications and inversions of $M \times M$ blocks.

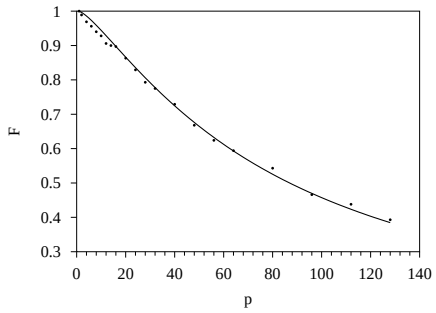

Fig. 6. Efficiency F as a function of the number p of processors. The dots correspond to the measured efficiency and the solid curve to the theoretical model employed.

The next step in our analysis is to perform a scaling size experiment. The aim of this test, is to scale the size of the problem such that the efficiency is kept fixed. As we saw from Eq. (8) the efficiency is independent of the size of the transversal dimension M and depends only on the size of the longitudinal dimension N and the number of processors p. Therefore, by scaling appropriately N with p it is possible to arrive at a fixed efficiency F of the algorithm. According to equation (9) for $p = 2$ processors the efficiency can be 0.848 if we choose $N = 8$. If we keep increasing the number of processors p and the size of the system N, keeping M fixed, according to the relation:

$$N' = N\frac{p' log_2(p')}{p log_2(p)}$$

where N' and p' are the new size of the system and the new number of processors respectively, then we expect that the efficiency will stabilize around 84.8%. Table 2 shows the efficiency for the scaled size problem.

We observe that the efficiency is stabilized between 0.81 and 0.85 thereby confirming our prediction. The sources of these slight deviations could be attributed to some enhanced contributions of time spent in interprocessor communications. Therefore our models provide a reliable source for the estimation

Table 2
Efficiency (F) as we increase the longitudinal dimension N of the billiard with the number of the processors p according to $N = O(plog_2(p))$. We keep $M = 100$ fixed.

$N; p$	T_s (sec)	T_p (sec)	F
$8; 2$	1.1	0.68	0.816
$32; 4$	4.76	1.44	0.826
$96; 8$	14.27	2.17	0.822
$256; 16$	38.32	2.82	0.849
$640; 32$	95.25	3.54	0.841
$1536; 64$	228.79	4.27	0.837
$3584; 128$	534.06	5.04	0.828
$8192; 256$	1222.07	5.82	0.82

of the computational cost. Table 2 shows that the larger the size of the system N, the larger becomes the efficiency. Therefore, our parallel algorithm is suitable for large systems, in particular of enhanced longitudinal dimension. Scattering problems with complex structures could be disentangled into modules with arbitrary complexity, of which the computation could be done efficiently by one processor. Cyclic reduction among the processors would join the information of the individual modules. If the computational complexity of a module is particularly enhanced for one processor, then more processors could be employed.

4.3 Antidot inside the scatterer

The second numerical benchmark corresponds to a category of scatterers with enhanced complexity. It consists of a Sinai billiard with a centered antidot of circular shape. This setup has been chosen for simulations in Ref. [14]. The numerical challenge imposed hereby is the exact reproduction of the antidot's circular shape in the continuum limit.

Figure 7 shows the discussed geometry. Subfigure 7-(a) shows the open geometry and dimensions of the Sinai billiard, while in 7-(b) the isolated Sinai billiard is discretized on a 49×49 grid of points. On such a small grid the antidot has, on the scale of Fig. 7-(b), the shape appearance of a polygon. Subfigure 7-(c) shows the same setup of the Sinai billiard but on a grid which is four times resolved compared to 7-(b), i.e., a 399×399 grid. The latter is going to be our fixed input size for the time measurements as we increase p. At

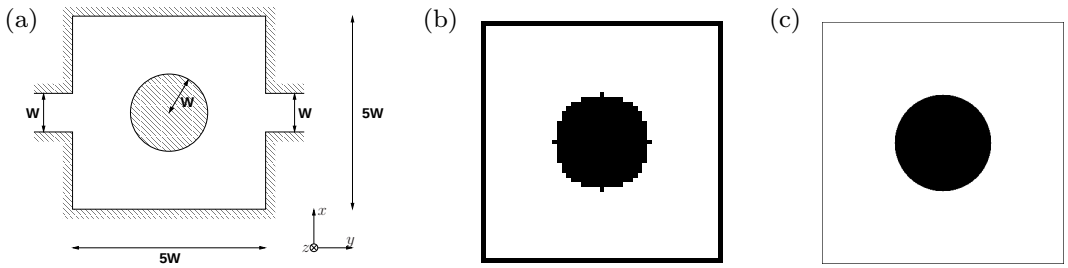

Fig. 7. (a) Open scattering geometry of a Sinai billiard with a centered antidot of circular shape. Subfigure (b) shows the isolated scatterer on a 49×49 grid of points and width $W = 10a$. Subfigure (c) shows the same setup but four times resolved. The thickness of the border lines in (b) and (c) provide a measure of the lattice constant.

this point we remark that the antidot has hard wall boundaries, i.e., the sites which form the antidot are excluded from the computation, thereby leading to blocks $\mathbf{A_{ij}}$ with varying dimensions. Table 3 shows the efficiency measured for the evaluation of $T(E)$ at a fixed energy E as a function of p.

Table 3
Measured time (Time) and efficiency (F) as a function of the number p of the processors for a Sinai billiard with an antidot placed centrally in it. The lattice $N = 399$ and $M = 399$ is kept fixed.

p	Time (sec)	$\_ F \_$	p	Time (sec)	$\_ F \_$	p	Time (sec)	$\_ F \_$
1	13490.83	1.0	14	1201.49	0.802	48	417.8	0.673
2	6791.23	0.993	16	1058.31	0.797	56	379.9	0.634
4	3917.2	0.861	20	855.45	0.789	64	343.87	0.613
6	2689.56	0.836	24	734.14	0.766	80	271.07	0.622
8	1974.65	0.854	28	655.5	0.735	96	267.04	0.526
10	1649.51	0.818	32	571.54	0.738	112	226.92	0.531
12	1404.99	0.800	40	462.83	0.729	128	224.37	0.47

The efficiency decreases with increasing p as expected. We should note that for these measurements equidistant domains, with respect to the longitudinal dimension, have been distributed among the processors. However, due to the antidot's boundaries, it becomes clear that this kind of distribution leads to an inevitable load imbalance. The domains that include sections of the antidot are described by blocks of smaller size, resulting thereby in reduced computational load for the corresponding processors. For $p = 2$, we observe an efficiency very close to 100%. This is a result of the symmetry of the geometry of the setup, which results in a load balanced problem for this specific number of processors. If we further increase p then the efficiency falls abruptly.

This result is attributed to the intensive load imbalance for few number of processors. To remedy this problem we have to choose a non-uniform domain decomposition of the scattering region, leading, thereby, to a more fair work load for all processors. For a larger number p, however, this problem becomes much less intense, since the total cost is multiply distributed in fairly small pieces of numerical load and the inequality among the processors, with respect to the load they share, significantly reduces. Therefore, for rather large p, load imbalance is not a significant source of parallel overhead, however, deviations compared to a load balanced setup are still evident (see below).

To analytically calculate the efficiency of the parallel algorithm for the setup in discussion, it is necessary to take into account the circular shape of the antidot. For this purpose, we divide the scatterer in two sections. One section of which the numerical cost scales with $N_1 \times M^3$ arithmetic operations, where N_1 the number of slices outside the antidot, and a second one of which its computational load scales with $\sum_{i=1}^{N_2} M_i^3$ where M_i is the varying size of the blocks of each of the N_2 slices that compose the antidot. Therefore, the size of the scattering problem is:

$$W(N, M) = 7N_1M^3 + 7\sum_{i=1}^{N_2} M_i^3$$

Moreover, we assume that at the first stage of parallelization, the work W is distributed uniformly among the processors and that at the second stage the processors that participate in the cyclic reduction are weighted appropriately, with respect to the load that corresponds to them. This is translated to the fact that $\frac{2}{5}p$ processors possess a work load that scales with $\sum_{i=1}^{N_2} M_i^3$ and $\frac{3}{5}p$ processors possess a work load that scales with M^3. Therefore, the cost for the parallel algorithm will be:

$$pT_p = 7N_1M^3 + 7\sum_{i=1}^{N_2} M_i^3 + 3plog_2(\frac{3p}{5})M^3 + 2plog_2(\frac{2p}{5})\sum_{i=1}^{N_2} M_i^3$$

The efficiency, which is no longer independent of the size of the transversal dimension M, will be:

$$F = \frac{W}{pT_p} = \frac{N_1M^3 + \sum_{i=1}^{N_2} M_i^3}{N_1M^3 + \sum_{i=1}^{N_2} M_i^3 + \frac{3}{7}p\,log_2(\frac{3p}{5})M^3 + \frac{2}{7}p\,log_2(\frac{2p}{5})\sum_{i=1}^{N_2} M_i^3} \qquad (10)$$

Figure 8 shows the measured efficiency (dots) as a function of p. We observe a rather abrupt decrease of F for a small number of processors $p > 10$ which

smoothens for larger p. The solid curve of Figure 8 represents the analytical model of Eq. (10), calculated for the 399×399 grid of subfigure (7)-c.

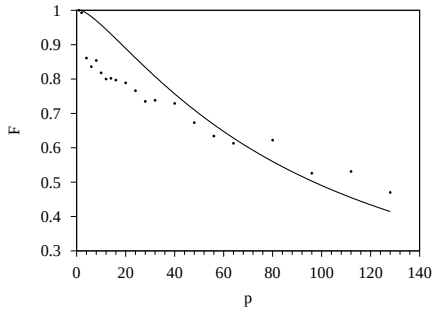

Fig. 8. Efficiency F as a funtion of the number p of processors. The dots correspond to the measured efficiency and the solid curve to the theoretical model derived to take into account the special geometry of the setup.

The agreement with the measurements is quite well, however, deviations for $p > 2$ are evident. For $p = 2$ the prediction agrees due to the symmetric load share to the two processors for this problem. For $p > 2$, deviations are apparent due to the assumptions within the derivation of our model. Namely, neither does W distribute itself evenly among the processors (load imbalance) nor is the computational load due to the cyclic reduction weighted exactly among the processors, as we assumed. To remove the first assumption one should proceed to an uneven domain decomposition with respect to the processors, which would vary depending on p. We conclude thereby, that in a scattering problem of complex geometry, the strategy to be followed in order to optimize the efficiency of the algorithm, regarding the load that the processors share, should take into account the particular geometric features of the scatterer.

5 Conclusions

A parallel algorithm for the implementation of the RGF method has been developed. The structure of the algorithm is mainly based on an initial domain decomposition of the scattering region due to processors' subdivision and recursive computation of the Schur's complement block through cyclic elimination of the processors. The computational cost due to the longitudinal dimension of the scattering region scales linearly with p. However, the cost due to the cyclic elimination, prevents us from achieving an efficiency of 100%. To demonstrate the efficiency of the parallel RGF algorithm, we proceeded with an analysis of the performance, scalability and sources of overhead for two specific numerical benchmarks. The first numerical benchmark corresponds to a perfectly load balanced setup, such as a Sinai billiard in a magnetic field, and the derived model is in very good agreement with the measurements. The second numerical example contained an additional geometrical challenge, being the exact reproduction of the circular shape of an antidot with hard wall

boundaries in the centre of a Sinai billiard. The computation hereby required manipulation of blocks with varying sizes leading to a nonuniform numerical load for the processors participating in the computation. A model adapted to the special geometry of this problem has been employed, which exhibited its geometric peculiarities and indicated the additional source of overhead due to load imbalance. The effect of the latter can be reduced by a selection of non-uniform decomposed domains distributed to the processors, based on the numerical cost. From our analysis it became apparent that the parallel RGF technique developed here, is particularly suitable for modular scattering structures of high complexity. Parallelization in this context gives the freedom to decompose the scatterer into modules, the computation of each can be efficiently performed by one processor. The optimized distribution of modules to processors depends on their individual complexity. In case, their complexity is enhanced, more than one processors could be employed and the corresponding computational load should be shared according to the individual features of the module.

P. S. D. and P. S. gratefully acknowledge illuminating discussions with G. Fagas. P. S. D. also acknowledges financial support from DFG in the framework of the International Graduiertenkolleg IGK 710 "Complex processes: Modeling, Simulation and Optimization".

References

[1] G. Moore, Cramming more components onto integrated circuits, *Electronics*, **38** (1965) 8

[2] S. Datta, *Electronic Transport in Mesoscopic Systems* (Cambridge University Press, 1995)

[3] R. Landauer, Conductance determined by transmission: probes and quantised constriction resistance,*J. Phys.: Condens. Matt.*, **1**, (1989) 8099–8110

[4] D.K. Ferry and S.M. Goodnick, *Transport in Nanostructures* (Cambridge University Press, 1997)

[5] S. Sanvito, C.J. Lambert, J.H. Jefferson and A.M. Bratkovsky, General Green's function formalism for transport calculations with *spd* Hamiltonians and giant magnetoresistance in Co- and Ni-based multilayers, *Phys. Rev. B*, **59** (1999) 11936–11948

[6] G. Fagas, *Vibrational Properties of Complex Solids*, PhD Thesis, (Lancaster University, 2000)

[7] H.R. Frohne, M.J. McLennan and S. Datta, An efficient method for the analysis of electron waveguides, *J. Appl. Phys.*, **66** (1989) 2699–2705

[8] S. Rotter, J.-Z. Tang,L. Wirtz, J. Trost and J. Burgdörfer, Modular recursive Green's function method for ballistic quantum transport, *Phys. Rev. B*, **62** (2000) 1950–1960

[9] G. Metalidis and P. Bruno, Green's function technique for studying electron flow in 2d mesoscopic samples, *arXiv:cond-mat/0411733* (2004)

[10] D. Mamaluy, M. Sabathil and P. Vogl, Efficient method for the calculation of ballistic quantum transport, *J. Appl. Phys.*, **93** (2003) 4628–4633

[11] D.S. Fisher and P.A. Lee, Relation between conductivity and transmission matrix, *Phys. Rev. B*, **23** (1981) 6851–6854

[12] E.F. Van de Velde, *Concurrent Scientific Computing* (Springer-Verlag, 1994)

[13] V. Kumar, A. Grama, A. Gupta and G. Karypis, *Introduction to Parallel Computing* (Benjamin-Cummings, 1994)

[14] N.G. Fytas, F.K. Diakonos, P. Schmelcher, M. Scheid, A. Lassl, K. Richter and G. Fagas, Magnetic-field dependence of transport in normal and Andreev billiards: a classical interpretation to the averaged quantum behavior, to appear in *Phys. Rev. B*